High-resolution transmission measurements for ^{54}Cr+n

R. F. Carlton and C. Baker
Physics & Astronomy Department, Middle Tennessee State University, Murfreesboro, Tennessee 37132, USA

J. A. Harvey
Oak Ridge National Laboratory, Oak Ridge, Tennessee 37830, USA

(Received 24 December 2005; revised manuscript received 30 August 2006; published 30 October 2006)

Neutron total cross-section measurements on ^{54}Cr up to a neutron energy of 2 MeV have been analyzed to deduce resonance parameters as well as spins and parities. Neutron strength functions have been deduced, based on data in the energy range 20–1000 keV, for s-, p-, and d-wave interactions and, in units of (10^{-4}), are 2.8±0.9, 0.23±0.06, and 4.4±0.7, respectively. Corresponding level densities in units of keV^{-1} are 0.025±0.003, 0.032±0.003, and 0.107±0.006, respectively. The distribution of nearest-neighbor spacings for s waves has been compared to Poisson and Wigner predictions for both ^{54}Cr and ^{52}Cr. Hints are seen of greater chaotic behavior in the case of the closed-neutron-shell ^{52}Cr and of regular dynamics for ^{54}Cr, suggestive of changes in chaoticity of nuclear dynamics with shell closure.

DOI: 10.1103/PhysRevC.74.044614 PACS number(s): 25.40.−h, 21.10.Ma, 21.10.Pc, 24.60.Lz

I. INTRODUCTION

Chromium has four stable isotopes (50, 52, 53, and 54) with respective percentage abundances (4.345, 83.789, 9.501, and 2.365). Neutron transmission measurements on all these isotopes have been performed at the Oak Ridge Electron Linear Accelerator (ORELA). Results for ^{52}Cr and ^{54}Cr, based on measurements performed at the 80-m flight path, were previously reported [1] in an investigation of the possible parity dependence of level densities at excitations as high as approximately 1 MeV. Oxide samples were used in both cases. These measurements represented a significant increase in energy resolution over previous studies, more than doubling the energy range of the analysis. This resulted in a notable revision of the strength function and level density values for s and p waves. First determinations [2,3] of the s-wave strength, based on low-resolution measurements up to a neutron energy of 400 keV, are well below that predicted by Mughabghab *et al*. [4] using a deformed optical model calculation. However, the work of Smith *et al*. [5] yielded predictions of the chromium s-wave strength function from spherical optical-, dispersive spherical optical-, and vibrational coupled-channels model calculations that were in reasonable agreement with Mughabghab's predictions. A summary of observed neutron resonance energies and widths prior to Agrawal *et al*. [1] listed only 31 total resonances up to a neutron energy of 400 keV [4]. The first ORELA data from the 80-m flight path extended the analysis to 900 keV and a total of 15 s-wave resonances and 95 non-s-wave resonances were observed in ^{54}Cr. In the present study we have identified 34 additional resonances for a total of 144 resonances (s: 23; p: 28; d: 93) in the energy range 20–950 keV.

The lightest and heaviest stable isotopes of chromium both differ by two neutrons from the magic number of 28 in ^{52}Cr. This provides for possible correlations of resonance properties with neutron shell structure near closed shells. In particular, any significant differences in level spacing or resonance width distributions could be suggestive of dynamically different systems. Their mass numbers place the chromium isotopes near the peak of the 3S giant resonance in a plot of the s-wave neutron strength versus mass number and in the minimum between the 2P and 3P peaks in a similar plot of p-wave neutron strength functions. This fortuity enhances the likelihood of obtaining a more complete set of pure s-wave resonances in a study of the present type. This in turn buttresses considerations of possible signatures of chaotic behavior in complex quantum systems in studies of individual nuclei as opposed to considerations of a whole body of available nuclear data [6].

The characteristics most easily and traditionally deduced from high-resolution neutron total cross-section measurements include the identification of the nuclear energy levels populated in the compound nucleus and the distributions of these levels and their associated widths. One of the measures used for the levels distribution is the nearest-neighbor spacing (NNS). An often-observed characteristic of the NNS distribution for nuclear states is spectral nonuniformity. This has served as a test of the ability of the Gaussian orthogonal ensemble (GOE) of asymptotically large real symmetric random matrices to predict such fluctuations, independent of the dynamics giving rise to the energy levels. In the early days these comparisons were through pure (same J^{π}) and complete (no missing levels) sequences of nuclear levels of individual nuclei [7]. As seen in that case, and generally, those NNS that are describable by random matrix theory (RMT) are characterized by level repulsion and spectral rigidity. The former reflects a tendency of the levels to avoid clustering and the latter a tendency of the spacings to be tightly distributed about their means, both implying correlations between levels. More recently, with mounting evidence that the GOE fluctuations are to be expected under very general conditions, and in view of the GOE taking into account no specific properties of the nuclear Hamiltonian, tests involving broad collections of levels, from many nuclei and several reaction types, still with the pure and complete requirements, have been used to further establish the applicability of the GOE, with greater statistical significance [8].

Wigner's pioneering work [9] in relating RMT to departures of nuclear energy levels from spectral uniformity has seen renewed and ongoing interest over the ensuing decades as similar patterns of behavior are seen in other complex systems such as Rydberg levels of an H atom in a magnetic field [10], elastomechanical eigenfrequencies of irregularly shaped quartz blocks [11], fluctuations of conductance of a small wire with magnetic field [12], and even in classically chaotic quantum systems with few degrees of freedom. In fact, the maturing of the field of RMT, with its attendant successes, has led to the expectation that fluctuations in generic quantum systems that follow RMT statistics of a suitably chosen ensemble result from an underlying dynamics that is chaotic. One expects, conversely, that when the classical dynamics is regular and integrable, the level statistics will follow the Poisson type. We raise the question of whether we can use the NNS distribution of an *individual* nuclide to reflect the underlying dynamics of a nuclear system. In pursuit of this question we have data for isotopes of chromium with neutron numbers at and beyond the magic number of 28. In the language of historical nuclear structure models, one expects that the internal dynamics changes with shell closure. Comparing the NNS distributions for these isotopes to GOE and Poisson predictions could provide answers. This is explored in the analysis to see if the distribution changes with shell closure. In Sec. II, we provide the experimental details, and in Sec. III we present the analysis of the data. In Secs. IV and V we describe the results and the extent to which neutron total cross section data on *individual* nuclei can signal chaotic nuclear dynamics.

II. EXPERIMENT

Neutron transmission measurements on a sample of $^{54}Cr_2O_3$ were performed at the ORELA [13,14] facility using the 200-m flight path. The 140-MeV pulsed electron beam provided 4-nsec neutron bursts with a continuous energy spectrum produced by the photoneutron process in the tantalum target and subsequent moderation in the 15-cm-diameter, beryllium-clad, water-filled target housing. Measurements employed the time-of-flight technique, using neutron pulses from the ORELA. The neutron energy resolution function is expressible by a combination in quadrature of the fluctuations in flight-path length and the burst width and has been determined to have a Gaussian shape with a full width at half maximum dE given in the present measurements by

$$\left(\frac{dE}{E}\right) = \sqrt{4 + 30E(\mathrm{MeV})} \times 10^{-4}.$$

Collimators were used both before and after the sample to select neutrons from only the Ta target. Overlap neutrons were eliminated by a 0.3-g/cm^2 ^{10}B filter. Gamma rays from the Ta target were reduced by a 1.095-cm-thick uranium filter 16.5 cm in diameter. A 0.712-cm-thick Pb filter, placed 5 m from the neutron source, covered the entire Ta target. Neutron detection occurred 201.568 m from the Ta target.

The oxide sample had a weight of 19.9615 g with percentage abundances of 95.40, 3.09, 0.18, and 1.33 of ^{54}Cr, ^{52}Cr, ^{50}Cr, and ^{53}Cr, respectively. The inverse Cr thickness of the $^{54}Cr_2O_3$ sample was 18.48 b/atom. The measurements did not provide for compensation for the oxygen in the sample, but correction was made for its presence, in the analysis, as discussed below. The sample was cycled, under computer control, into and out of the beam at a position 9 m from the Ta target with a cycle time of approximately 20 min and 14 min, respectively. At this position, the neutron beam was collimated to a diameter of 2.38 cm. Data were "dumped" daily and these individual runs were combined and the resulting data were corrected for dead time. A neutron monitor was placed in the neutron beam of another flight path to permit compensation for fluctuations in the neutron production rate during the 7-day period over which 144 h of data were collected. Neutrons were detected from the proton recoils as they traversed a 2.54-cm thickness of a 5.2 cm × 8.9 cm piece of NE110 scintillator. With the scintillator optically coupled to two RCA 8854 photomultiplier tubes the efficiency for the detection of neutrons up to 2 MeV was approximately 70%. Additional experimental details relating to the ORELA facility and its use in measuring high-resolution neutron tranmissions are found in technical reports [15]. More detailed discussions of corrections for various backgrounds in ORELA data are discussed in Ref. [16]. After these corrections, the transmission was computed from the sample-in-to-sample-out ratio and normalized to the corresponding neutron monitor counts. Before beginning the resonance analysis, the transmission data were averaged to reduce the number of data points in regions absent of structure and thus speed calculations.

III. ANALYSIS

Because the oxygen in the sample was not compensated in the transmission measurements, its presence in the computed cross section is unmistakable at those energies where large resonances occur in oxygen, as seen at 434 keV in Fig. 1. We have compensated for the presence of oxygen, in the analysis, by including in the parameter file resonance parameters for

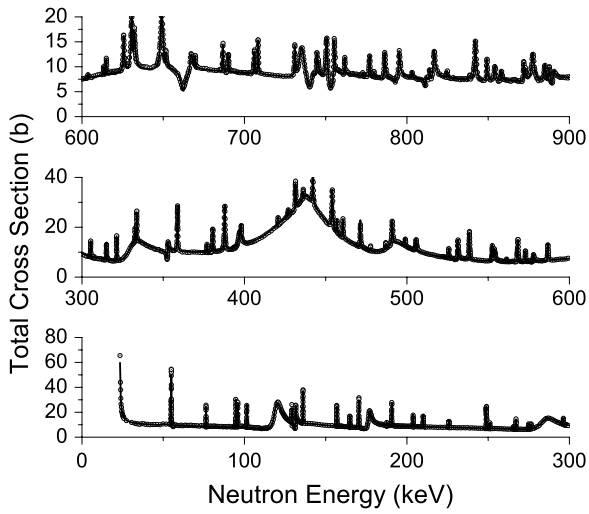

FIG. 1. Total neutron cross section for n+^{54}Cr. The solid line gives the R-matrix representation of the data based on our deduced resonance parameters.

all the spin groups and resonances necessary to describe the total cross section of ^{16}O. These resonance parameters have been accurately determined [17] from an R-matrix analysis of a careful measurement of the ^{16}O total cross section and held fixed during the R-matrix analysis we used to deduce the energies and widths of the resonances due to ^{54}Cr. Despite the high quality of the oxygen measurement and analysis, this method of compensation increases the uncertainty of deduced ^{54}Cr resonance widths but only in the vicinity of significant oxygen resonances.

The averaged transmission data were analyzed using the Reich-Moore formulation of the R-matrix theory [18]. The full character of the data cannot be represented from just the R-matrix parameters of resonances that are visible in the energy region of analysis. This is due to the fact that other unobserved resonances outside the region bear an imprint on the spectrum. These so-called external resonances provide a general background contribution and also impact the resonance-resonance interference asymmetry. These contributions have been parametrized, for each spin group, through a logarithmic R function that captures these background and interference influences while at the same time permitting ease of comparison with predictions of an optical model. It is also possible to use so-called dummy resonances that individually provide for the collective influence of many external resonances. The resonance set for the oxygen resonances [17], in fact, uses this approach and are a part of the total parameter file in the present study. For representing the influences of external resonances, we use the logarithmic R-function description for chromium and dummy resonances for oxygen.

We have used a fixed channel radius of 5.48 fm for all the chromium spin groups and 3.79 fm for oxygen. In the fitting process calculated transmission resonances are resolution broadened and converted to cross section for Doppler broadening before comparison with the data. An effective nuclear temperature of 300 K has been used in the Doppler broadening. From Fig. 1 we see a number of relatively broad resonances having an asymmetry characterizing the s-wave interaction. These are generally unambiguous by their peak height, width and shape, but in some instances broad $p_{1/2}$ resonances may appear as s waves because of their same peak height, as in the case of the broad resonance just below 400 keV in Fig. 1. A notable s-wave resonance is seen at 600 keV, whose width of 100 keV is six times that of any other ^{54}Cr resonance in the entire spectrum.

We have partitioned all resonances into spin and parity groups up to and including $\frac{5}{2}^+$ on the basis of χ^2 comparisons of fitted results for different assumed J^π. This has been accomplished through the spin group variation feature of the code RSAP [19] that invokes the program SAMMY [18] sequentially for each assumed spin and parity. Although there may be ambiguity in the spin assignment of narrow resonances within a p- or d-wave parity group, the parity assignments are more definite. This is a result of the very different shapes of resonances having differing orbital angular momentum. Although $s_{1/2}$ and $p_{1/2}$ resonances have the same maximum peak height, their shapes (or asymmetries) can be and usually are very different. The same can be said for $p_{3/2}$ and $d_{3/2}$. This is illustrated later, for s- and p-wave resonances, in discussions regarding the purity of our s-wave sample. A more complete description of the R-matrix fitting of neutron total cross-section data from ORELA is seen in Ref. [20], Sec. III B, and Fig. 4 in particular.

IV. RESULTS

We have observed a total of 330 resonances up to a neutron energy of 2 MeV. Previous transmission studies did not resolve resonances above 900 keV. Agrawal *et al*. [1] reported 110 resonances up to that energy. The present analysis reveals 131 over the same energy range. The present work has sufficient resolution to enable distinction between p-wave and d-wave resonances. The work of Agrawal *et al*., however, treated non-s-wave resonances as being due to p-wave interactions and speculated on a parity dependence in level densities. We find that approximately 70% of the resonances observed up to 900 keV actually result from d-wave interactions. We thus present average results (strength functions and level densities) for s-, p-, and d-wave interactions. Due to the decreased certainty of our parity groupings above 1 MeV, we report the results of our analysis for both of these upper energy limits, with the 2 MeV results in braces.

A. s waves

We observed a total of 25 {55} resonances over the respective energy ranges, compared to the 15 seen by Agrawal *et al*. up to 900 keV. These resonances are clearly distinguished by their asymmetry resulting from resonance-resonance and resonance-potential scattering interference. Examples are seen in Fig. 1 at 120, 280, and 330 keV. Small s-wave resonances in proximity to larger ones, like those at 350 and 670 keV, manifest a different asymmetry due to resonance-resonance interference. The s-wave group is thus the purest of the three.

Histogram plots of the cumulative reduced neutron width and the cumulative number of resonances, with linear fits, are shown in Fig. 2. The slopes of linear fits to these plots represent the strength function and level density, respectively.

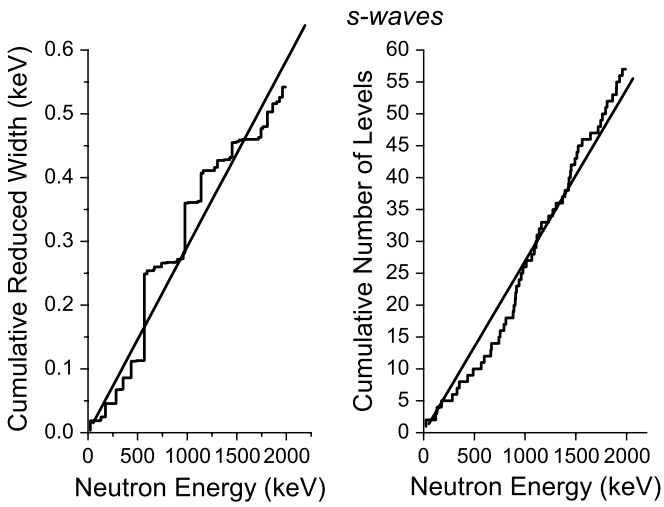

FIG. 2. Cumulative reduced widths and cumulative number of resonances for n+^{54}Cr s waves. The slopes represent the s-wave strength and level density, respectively.

One can see from the strength plot that somewhat different slopes obtain for different energy segments, being relatively low ($\sim 2.0 \times 10^{-4}$) in the ranges 0–600 keV and 1250–2000 keV and $\sim 3.0 \times 10^{-4}$ in the intervening region. Because these values are within the uncertainties, we have shown only the fit to the entire energy range. Despite the pronounced increase in cumulative reduced width near 600 keV, a doorway state hypothesis does not seem justified when viewed in the context of the whole. In fact the values, over either of the energy ranges, are consistent with that of Agrawal *et al*. despite the much smaller number of observed resonances in that study. The strength functions for the 25 {55} resonances (in units of 10^{-4}) are 2.8±0.9 {2.5±0.5} and the level densities (in units of keV^{-1}) are 0.025±0.003 {0.027±0.002}. The presented uncertainties are not associated with missing or misassigned levels but are reflective of the statistical errors associated with the determination of the mean reduced neutron width and the mean level spacing [21]. The values of each parameter, over the two energy ranges, are within uncertainties and least-squares fits over the two energy ranges are almost indistinguishable, for both plots. Although the J^π assignments above 1000 keV are less certain than those below, our conclusions would not be changed if only considering the more assured J^π values. Due to the resonances at 434, 667, 881, and 889 keV that were not reported by Agrawal *et al*., our level density, based on resonances up to 1000 keV, is 32% greater. The value reported by Mughabghab, based on resonances up to 400 keV, was lower than Agrawal by 58%. Both of these differences are greater than the reported uncertainties. The resonance parameters for indentified *s*-waves are shown in Table I. Resonance parameters for other partial waves will be transmitted to the National Nuclear Data Center at Brookhaven National Laboratory.

TABLE I. *s*-wave resonance parameters (energy and neutron width) deduced from neutron total cross sections for n+^{54}Cr. [In our notation 22.987(5) means 22.987±0.005.]

E_n (keV)	Γ_n (keV)	E_n (keV)	Γ_n (keV)	E_n (keV)	Γ_n (keV)
22.987(5)	0.56(2)	902.8(5)	0.23(3)	1392.5(9)	0.27(5)
119.23(3)	5.09(4)	908.0(5)	3.0(2)	1429(1)	0.7(1)
131.46(4)	0.31(1)	915.6(5)	0.22(3)	1434(1)	1.9(2)
176.46(5)	2.06(2)	941.6(5)	0.33(5)	1448(1)	0.43(8)
283.4(1)	11.1(1)	961.0(6)	1.0(1)	1453(1)	0.9(1)
329.6(1)	12.3(1)	977.7(6)	10.6(3)	1491(1)	25(1)
352.8(1)	0.44(2)	1003.9(6)	38.3(7)	1510(1)	0.7(1)
434.4(2)	12.0(2)	1037.5(6)	26.0(5)	1523(1)	1.1(2)
487.6(2)	18.1(2)	1065.9(6)	0.46(6)	1562(1)	1.3(2)
567.8(3)	0.47(6)	1091.7(7)	0.29(4)	1718(1)	1.6(3)
596.3(3)	102(1)	1107.5(7)	0.21(4)	1764(1)	4.8(8)
663.1(3)	3.9(1)	1117.1(7)	2.4(2)	1794(1)	4.0(6)
667.5(3)	2.1(2)	1140.3(7)	0.31(6)	1801(1)	1.1(2)
741.0(4)	3.4(2)	1161.3(7)	55(1)	1858(1)	28(3)
753.8(4)	5.2(2)	1231.4(8)	6.6(4)	1902.9(9)	1.1(2)
793.0(4)	0.10(2)	1274.0(8)	0.18(4)	1903(1)	18(2)
811.6(4)	0.39(4)	1305.8(9)	5.6(4)	1930(2)	3.4(6)
881.2(5)	0.10(2)	1369.5(9)	14.2(7)	1989(2)	6.6(9)
889.8(5)	1.07(8)				

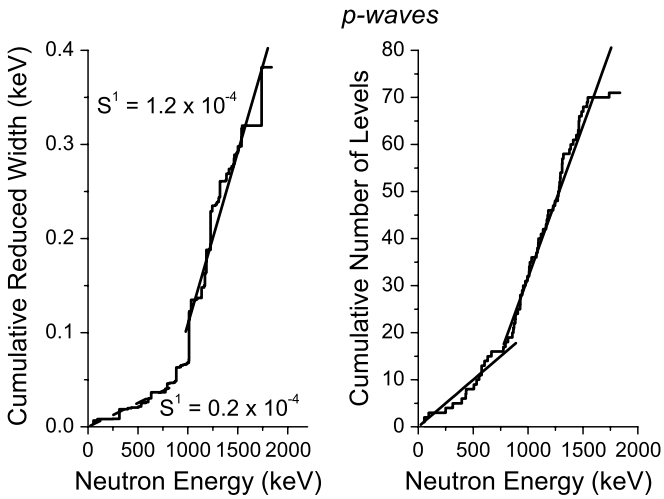

FIG. 3. Cumulative reduced widths and cumulative number of resonances for n+^{54}Cr p waves. The slope of the former gives (2λ + 1) times the strength and that of the latter gives the level density. Marked changes are noted in the strength and level density at a neutron energy of 1 MeV.

B. *p* waves

Agreement with earlier results ends with the discussion of *s* waves, due to Agrawal's previously mentioned assignment of negative parity to all other resonances. In the present analysis there is sufficient difference, at these energies, in the character of the resonance-potential scattering interference that, for *p* and *d* waves, distinctive asymmetry differences result. As a result we have identified 31 {72} resonances that correspond to *p*-wave interaction. In Fig. 3 it is clear that a sharp, sixfold increase in the cumulative reduced width occurs at 1000 keV. The line segments represent least-squares fits to the data in the two corresponding energy ranges. The strengths corresponding to these lines can be deduced from the slopes, reduced by the factor 2λ + 1, where λ is the orbital angular momentum quantum number. Unlike the case for *s* waves where there are several step increases in the cumulative reduced neutron width but yet the average results are almost the same for the two energy ranges, the *p* waves present a sustained increase of strength, possibly related to intermediate nuclear structure in the ^{55}Cr nucleus at this excitation energy. Agrawal reported a similar dramatic increase in strength, but with the step occurring at 350 keV instead of the 1000 keV observed here. However, the similarity must be accidental because the former work lumped all non-*s*-wave resonances in the *p*-wave category. The *p*-wave strength function deduced from these resonances accords with expectations based on spherical optical model predictions [22]. ^{54}Cr is in the mass region where the *s*-wave strengths are near a maximum of 3–4 $\times 10^{-4}$ and the *p*-wave strengths are a factor of 10 smaller. Our values of 0.23±0.06 $\{0.89\pm0.16\}\times10^{-4}$ differ from the *s*-wave values by factors of 12 and 3, respectively. The level densities for *p*-waves are 0.032±0.003 {0.040± 0.002} keV^{-1}. From Fig. 3 it can be seen that the slope of the level density plot over the energy range 1000 to 2000 keV is double that up to 1000 keV, the abrupt change occurring at

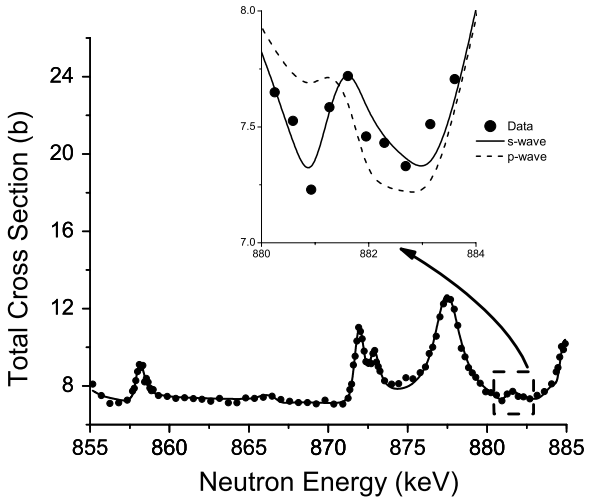

FIG. 4. R-matrix fit to a region containing s- and p-wave resonances at the experimental detection limit, showing that the s-wave sample does not contain spurious p waves.

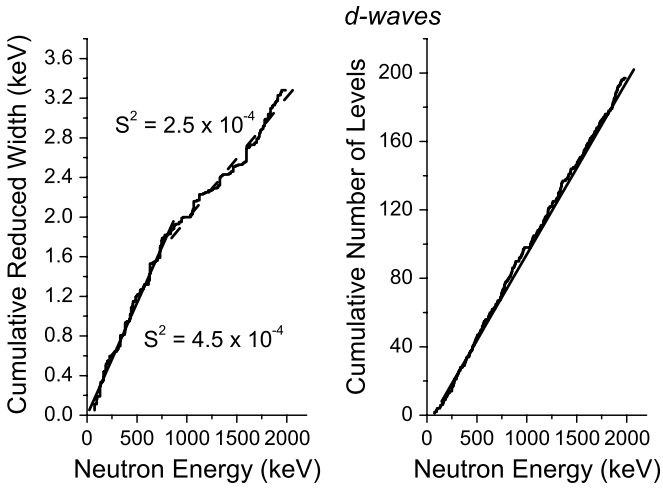

FIG. 5. Cumulative reduced widths and cumulative number of resonances for n+^{54}Cr d waves. The slope of the former gives $(2\lambda + 1)$ times the strength and that of the latter gives the d-wave level density.

the same energy as in the strength plot. This may strengthen support for nuclear structure effects for the p-wave interaction.

It is worthy of note that the numbers of s- and p-wave resonances do not accord with statistical expectations. One explanation is that the s-wave sample has been poisoned with misassigned p waves. For the p:s ratio to accord with the expected 3:1 statistical ratio, 11 of the s-wave assignments would have to be wrong, assuming all d-wave assignments are correct. The unlikelihood of this "poisoning" hypothesis is seen in Fig. 4, where we show a region containing both s- and p-wave resonances that are among the smallest we can observe. The R-matrix fits [see inset] corresponding to s- and p-wave assumptions for the resonance at 882 keV show clearly by the solid and dashed lines, respectively, that if we can see a resonance we can conclusively distinguish its parity. It is clear that this s-wave and the p-wave resonance at 866 keV, which are at our detection limit, require different resonance asymmetries to fit the data. This increases the confidence that the s-wave population is pure. The other possible explanation for the p:s ratio is that if we have missed some s-wave resonances, we have missed considerably more p waves. That possibility has been explored using the Fuketa-Harvey method [23] of estimating missed resonances in neutron total cross-section data, as applied in Ref. [24]. We do find more missed p waves but not enough more to bring the ratio to the expected value. We find at most 2 s waves and 9 p waves could have been missed, corresponding to a p:s ratio of 1.5:1. The impact of missed resonances on the calculated strength is less than 0.5% for the p-wave strength and negligible for s waves. The impact upon level spacings is 8% for s waves and 23% for p waves.

C. *d* waves

The d-wave interaction has the greatest strength of the three partial waves in addition to revealing more resonances than the other two interactions combined, having totals of 97 {203}. The trends for the cumulative number of resonances in the two energy ranges are indistinguishable so only that for the entire energy range is plotted in Fig. 5. The level densities over the defined energy ranges are 0.107±0.006 {0.105± 0.004} keV^{-1}. The linearity of level density over the entire range gives added confidence in the assignment of resonances to that spin group. For the cumulative reduced width plot we have shown separate least squares fits to the two energy regions to show the diminution of strength above 1000 keV, at the point where we saw a notable increase of strength for the p-wave group over that energy range. As in the case of p waves, the strength function is deduced from the slope, reduced by the factor $2\lambda + 1$, where λ is the orbital angular momentum quantum number. The evaluated d-wave strengths are 4.4±0.7 $\{3.8\pm0.4\}\times10^{-4}$, in agreement with Mughabghab [22] and 50% greater than the strength for s waves.

D. *R* functions

In addition to the level spacings and strength functions, the resonance analysis enables us to deduce the parameters of the external R functions. This is possible through fitting of the resonance-potential scattering interferences for each individual partial wave. This interference is manifest in the resonance asymmetry for the larger resonances. In general the extent of asymmetry diminishes with increasing angular momentum quantum number. The R function, for a given partial wave, is a linearly increasing function of neutron energy and is an alternative means of accounting for the contributions, within the analyzed region, due to resonances outside the analyzed energy range. The alternative to this approach is to use dummy resonances whose energies are outside the analyzed region. The former approach has the advantage of simplifying comparisons with optical model calculations of average properties of the interaction. The R function has the form,

$$R_{\ell J}(E) = \alpha_{\ell J} + \beta_{\ell J} E - \tilde{s}_{\ell J} \ln\left(\frac{E_{\rm up} - E}{E - E_{\rm lo}}\right),$$

where $\tilde{s}$ is the external strength and α and β are constants determined by the least-squares analysis. We find that the

TABLE II. Average resonance parameters for $n+^{54}$Cr, based on the analysis up to 1000 keV. The average level spacings, $\bar{D}$, do not include corrections for missed resonances discussed above in Sec. IV B. In our notation, 40(4) is equivalent to 40±4; 2.8(9) is equivalent to 2.8±0.9.

ℓ_J	Num	$\bar{D}_{\ell J}$ (keV)	$S^{\ell}_{J}(\times 10^{-4})$	$\alpha_{\ell J}$	$\beta_{\ell J}$ $(\mathrm{MeV})^{-1}$	$\tilde{s}_{\ell J}$
$s_{\frac{1}{2}}$	25	40(4)	2.8(9)	0.111(5)	0.08(1)	0.13(4)
$p_{\frac{1}{2}}$	10	102(18)	0.3(2)	−0.65(4)	1.9(2)	0.029(9)
$p_{\frac{3}{2}}$	21	37(4)	0.20(7)	−1.0(1)	1.2(1)	0.016(4)
$d_{\frac{3}{2}}$	51	18(1)	6(1)	−0.63(8)	0.32(6)	0.16(3)
$d_{\frac{5}{2}}$	46	19(2)	3.7(8)	0.002	0.0	0.16(3)
p	31	31(3)	0.23(6)			
d	97	9.3(5)	4.4(7)			

external strengths needed are energy independent and have taken the values to be equal to the strengths in the analyzed region, for each partial wave. This external R function then becomes an additive term in the total R function of the R-matrix formalism. This approach has been discussed more extensively elsewhere [25]. The parameters deduced for each partial wave are presented in Table II.

V. HINTS OF QUANTUM CHAOTICITY IN THE CR COMPOUND NUCLEUS

Whether nuclear energy level spectra display uniformity may suggest whether the associated dynamics is regular or chaotic. In general, the spectra of nuclear levels with the same quantum numbers have been found to display fluctuations from uniformity, with the spacing of adjacent levels being tightly grouped about the mean and manifesting repulsion effects. Distributions for the NNS for a broad collection of low-lying nuclear levels having well-established quantum numbers have been generally well described [26] by the Wigner distribution,

$$P(s) = A \cdot s \cdot e^{-\pi(s^2/4)},$$

which can be derived from the GOE of random-matrix theory. Such is also expected to be the case for quantum systems for which the underlying dynamics are chaotic. Conversely, if the underlying dynamics are nonchaotic, the NNS distribution should more nearly reflect the character of independent random variables of a Poisson sample. One expects therefore that the statistics of energy level spacings will be typically described either by random matrix theory, when the classical limit is chaotic, or by a Poisson process when the classical dynamics are regular, i.e., completely integrable. Therefore nuclear level fluctuations such as these are understood and interpreted in the framework of random-matrix theories. The Wigner representation of a NNS distribution for ^{166}Er is seen in Fig. 6, where the number, of a total of 172 levels, populated by s-wave neutron interaction with ^{166}Er nuclei is plotted as a function of the spacing, s, normalized by the average spacing. ^{166}Er was chosen because of the large and pure (same J^{π}) sample of levels [27] available and the fact that the nucleus is not near a magic number for either type of nucleon. The peak in the distribution manifests the rigidity (nonuniformity) of the

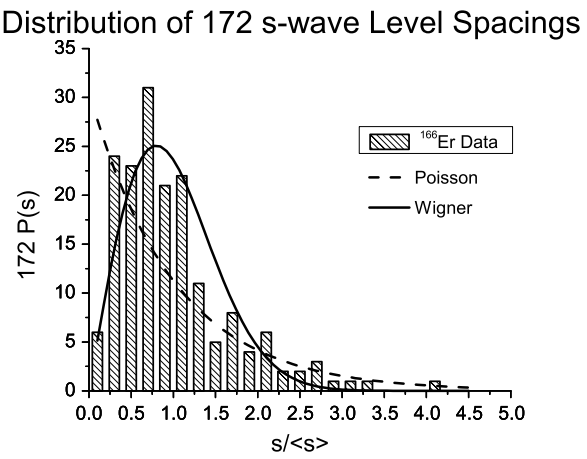

FIG. 6. s-wave NNS distribution representing a large pure sample of level spacings. The agreement of the Wigner distribution with the ^{166}Er data suggests an underlying chaoticity in the nuclear dynamics.

distribution and the repulsion between levels is seen in the low number of small spacings observed.

The Wigner fit represents the distribution well. It is clear from the figure that the small number of levels with small spacings would not be well represented by the Poisson distribution, suggesting complexity in the nuclear dynamics of ^{166}Er—a complexity consistent with the chaoticity in the fluctuation properties of the compound nucleus model. We previously reported [28] on results of an R-matrix analysis of the total neutron cross section for $n+^{52}$Cr, where we identified 28 s-wave resonances. In Fig. 7 we present results of a similar comparison of Wigner and Poisson representations of the NNS distribution for the case of this nucleus with a magic number of neutrons. This distribution too is seen to be best described by the statistics of random matrix theory.

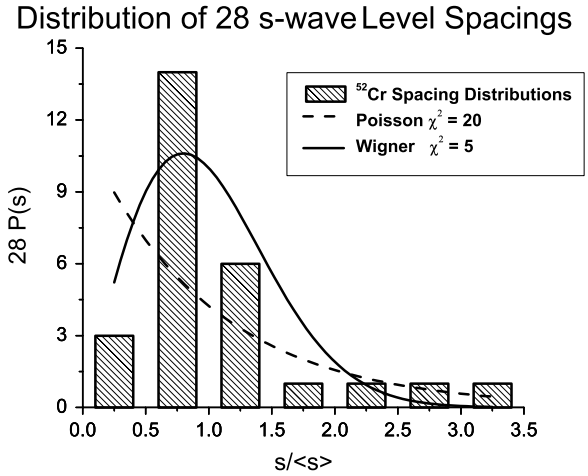

FIG. 7. Nearest-neighbor spacing distribution for the closed-neutron shell of ^{52}Cr. The χ^2 values suggest a Wigner distribution for the 28 NNS.

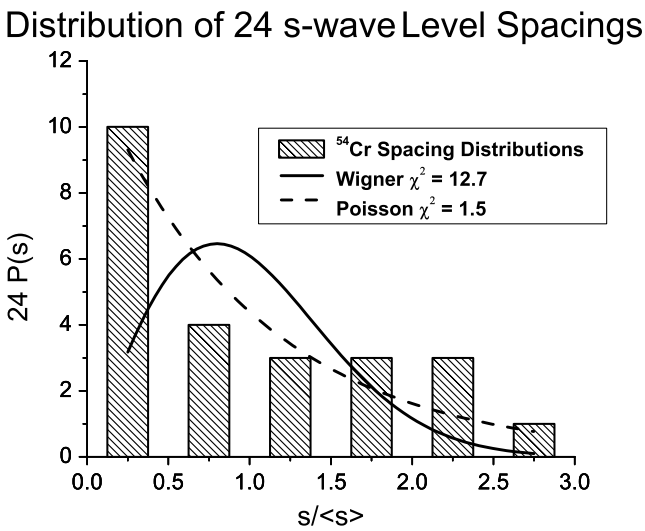

FIG. 8. Nearest-neighbor spacing distribution for the case of two neutrons outside a closed neutron shell in ^{54}Cr. The χ^2 values suggest a Poisson distribution for the 24 NNS.

For the case of ^{54}Cr we find the opposite to be true as seen in Fig. 8, where the distribution of the NNS for the 25 resonances observed in the $n+^{54}$Cr reaction is better described by the Poisson distribution of the form,

$$P(s) = A \cdot e^{-s},$$

where A is the parameter adjusted to fit the distribution. This statistic characterizes the behavior of systems whose equations of motion are integrable. One can ask whether for *individual* nuclei the spectral nonuniformity can be used as an indicator of chaoticity, because of the cases presented, the one with single or independent particle character reflects a Poissonian NNS distribution.

As mentioned, the purity of the sample is of critical importance. For the cases of chromium, this is aided by the wide disparity of the strength functions for s- and p-wave neutrons in the region, $A = 50$, ensuring a reduced likelihood of p-wave contamination of the s-wave sample. In addition, the tendency for s and d waves to manifest asymmetric resonances or not, respectively, further assures the purity of the sample of s-wave resonances. Similar study of other chromium isotopes or other nuclei having several stable isotopes would shed additional light on the question of any connection of NNS distributions of *individual* nuclei with quantum chaoticity.

ACKNOWLEDGMENTS

This research was sponsored by the Basic Energy Sciences Division of the U.S. Department of Energy under contract DE-FG05-86ER40293 with Middle Tennessee State University. Oak Ridge National Laboratory is managed by UT-Battelle, LLC for the U.S. Department of Energy under contract DE-AC05-00OR22725.

[1] H. M. Agrawal, J. B. Garg, and J. A. Harvey, Phys. Rev. C **30**, 1880 (1984).
[2] J. A. Farrell, E. G. Bilpuch, and H. W. Newson, Ann. Phys. (NY) **37**, 367 (1966).
[3] G. Stieglitz, R. W. Hockenbury, and R. C. Block, Nucl. Phys. **A163**, 5912 (1971).
[4] S. F. Mughabghab, M. Divadeenam, and N. E. Holden, *Neutron Cross Sections* (Academic Press, New York, 1981), Vol. 1, Part A.
[5] A. B. Smith and D. Schmidt, J. Phys. G **23**, 197 (1997).
[6] O. Bohigas, M. J. Giannoni, and C. Schmit, Phys. Rev. Lett. **52**, 1 (1983).
[7] H. I. Liou, H. S. Camarda, S. Wynchank, M. Slagowitz, G. Hacken, F. Rahn, and J. Rainwater, Phys. Rev. C **5**, 974 (1972).
[8] T. Guhr, A. Müller-Groeling, and H. A. Weidenmüller, Phys. Rep. **299**, 190 (1998).
[9] E. P. Wigner, Ann. Math. **53**, 36 (1951); Ann. Math. **62**, 548 (1955); SIAM Rev. **9**, 1 (1967).
[10] D. Wintgen and H. Friedrich, Phys. Rev. A **35**, 1464 (1987).
[11] C. Ellegaard, T. Guhr, K. Lindemann, J. Nygard, and M. Oxborrow, Phys. Rev. Lett. **77**, 4918 (1996).
[12] S. Washburn and R. A. Webb, Adv. Phys. **35**, 375 (1986).
[13] J. A. Harvey and N. W. Hill, Nucl. Instrum. Methods **162**, 507 (1979).
[14] C. M. Perey, J. A. Harvey, R. L. Macklin, F. G. Perey, and R. R. Winters, Phys. Rev. C **27**, 2556 (1983).
[15] D. C. Larson, N. M. Larson, J. A. Harvey, N. W. Hill, and C. H. Johnson, Oak Ridge National Laboratory Report No. ORNL/TM-8203, Oak Ridge, Tennessee, 1983 (unpublished); D. C. Larson, N. M. Larson, and J. A. Harvey, Oak Ridge National Laboratory Report No. ORNL/TM-8880, Oak Ridge, Tennessee, 1984 (unpublished).
[16] R. R. Winters, R. F. Carlton, C. H. Johnson, N. W. Hill, and M. R. Lacerna, Phys. Rev. C **43**, 492 (1991).
[17] L. C. Leal, R. O. Sayer, N. M. Larson, and R. R. Spencer, Trans. Am. Nucl. Soc. **79**, 175 (1998).
[18] N. M. Larson, Updated Users' Guide for SAMMY, ORNL/TM-9179/R6, Oak Ridge National Laboratory, 2003 (unpublished); N. M. Larson, Introduction to the Theory and Analysis of Resolved (and Unresolved) Neutron Resonances via SAMMY, ORNL/TM-6576, Oak Ridge National Laboratory, 1998 (unpublished).
[19] R. O. Sayer, Oak Ridge National Laboratory Report No. ORNL/TM-2001/15, Oak Ridge, Tennessee, 2001 (unpublished).
[20] R. F. Carlton, R. R. Winters, C. H. Johnson, N. W. Hill, and J. A. Harvey, Phys. Rev. C **38**, 1605 (1988).
[21] J. E. Lynn, *The Theory of Neutron Resonance Reactions* (Clarendon Press, Oxford, England, 1968).
[22] S. F. Mughabghab, in *Proceedings of the Third Conference on Neutron Cross Sections and Technology Knoxville, Tennessee, 1971*, edited by J. A. Harvey and R. L. Macklin, CONF 710301 (U.S. AEC Division of Technical Information Extension, Oak Ridge, Tenn., 1971), p. 386.

[23] T. Fuketa and J. A. Harvey, Nucl. Instrum. Methods **33**, 107 (1965).
[24] R. L. Macklin, J. Halperin, and R. R. Winters, Nucl. Sci. Eng. **71**, 182 (1979).
[25] C. H. Johnson, C. Mahaux, and R. R. Winters, Phys. Rev. C **32**, 359 (1985); C. H. Johnson and R. R. Winters, Phys. Rev. C **21**, 2190 (1980).
[26] J. F. Shriner, G. E. Mitchell, and T. von Egidy, Z. Phys. A **338**, 309 (1991).
[27] S. F. Mughabghab, *Neutron Cross Sections* (Academic Press, New York, 1984), Vol. 1, Part B.
[28] R. F. Carlton, J. A. Harvey, D. C. Larson, and N. W. Hill, Phys. Rev. C **62**, 014608 (2000).